Effect of Eu doping and partial oxygen isotope substitution on magnetic phase transitions in $(Pr_{1-y}Eu_y)_{0.7}Ca_{0.3}CoO_3$ cobaltites

N. A. Babushkina,[1] A. N. Taldenkov,[1] S. V. Streltsov,[2,3] T. G. Kuzmova,[4]
A. A. Kamenev,[4] A. R. Kaul,[4] D. I. Khomskii,[5] and K. I. Kugel[6]

[1] *National Research Center "Kurchatov Institute", Kurchatov Square 1, Moscow, 123182 Russia*
[2] *Institute of Metal Physics, Ural Branch, Russian Academy of Sciences, S. Kovalevskaya Str. 18, Ekaterinburg, 620990 Russia*
[3] *Ural Federal University, Mira Str. 19, Ekaterinburg, 620002 Russia*
[4] *Department of Chemistry, Moscow State University, 119991 Moscow, Russia*
[5] *II. Physikalisches Institut, Universität zu Köln, Zülpicher Str. 77, 50937 Köln, Germany*
[6] *Institute for Theoretical and Applied Electrodynamics, Russian Academy of Sciences, Izhorskaya Str. 13, Moscow, 125412 Russia*

(Dated: January 11, 2013)

We study experimentally and theoretically the effect of Eu doping and partial oxygen isotope substitution on the transport and magnetic characteristics and spin-state transitions in $(Pr_{1-y}Eu_y)_{0.7}Ca_{0.3}CoO_3$ cobaltites. The Eu doping level y is chosen in the range of the phase diagram near the crossover between the ferromagnetic and spin state transitions ($0.10 < y < 0.20$). We prepared a series of samples with different degrees of enrichment by the heavy oxygen isotope ^{18}O, namely, containing 90%, 67%, 43 %, 17 %, and 0 % of ^{18}O. Based on the measurements of ac magnetic susceptibility $\chi(T)$ and electrical resistivity $\rho(T)$, we analyze the evolution the sample properties with the change of Eu and ^{18}O content. It is demonstrated that the effect of increasing ^{18}O content on the system is similar to that of increasing Eu content. The band structure calculations of the energy gap between t_{2g} and e_g bands including the renormalization of this gap due to the electron-phonon interaction reveal the physical mechanisms underlying such similarity.

PACS numbers: 72.80.Ga, 75.30.Wx, 32.10.Bi, 71.27.+a, 71.15.Mb, 75.25.Dk

I. INTRODUCTION

Most magnetic oxides are characterized by a strong interplay of electron, lattice, and spin degrees of freedom giving rise to multiple phase transitions and different types of ordering. The phase transitions are often accompanied by the formation of different inhomogeneous states. In such situation, the oxygen isotope substitution provides a unique tool for investigating inhomogeneous states in magnetic oxides, which allows studying the evolution of their properties in a wide range of the phase diagram. Sometimes, particularly if a system is close to the crossover between different states (usually leading to a phase separation), the isotope substitution can lead to significant changes in the ground state of the system.[1].

A good example of such phenomena is provided by cobaltites. These perovskite cobalt oxides have attracted a special interest owing to the possibility of the spin-state transitions (SST) for the Co ions induced by temperature or doping[2–8] and the related phase separation phenomena.[9–16] The effect of $^{16}O \rightarrow ^{18}O$ isotope substitution on the properties of $(Pr_{1-y}Eu_y)_{0.7}Ca_{0.3}CoO_3$ cobaltites ($0.12 < y < 0.26$) was studied earlier in our paper Ref. 17. It was found that with increasing Eu content, the ground state of the compound changes from a "nearly-metallic" ferromagnet (ferromagnetic metallic clusters embedded into an insulating host) to a "weakly-magnetic insulator" at $y < y_{cr} \approx 0.18$, regardless the isotope content. A pronounced SST was observed in the insulating phase (in the samples with $y > y_{cr}$), whereas in the metallic phase (at $y < y_{cr}$), the magnetic properties were quite different, without any indications of a temperature-induced SST. Using the magnetic, electrical, and thermal data, we constructed the phase diagram for this material. The characteristic feature of this phase diagram is a broad crossover range near y_{cr} corresponding to a competition of the phases mentioned above. The $^{16}O \rightarrow ^{18}O$ substitution gives rise to an increase in temperature T_{SS} of the SST and to a slight decrease in the ferromagnetic (FM) transition temperature T_{FM}.

However, a number of problems important for understanding the physics of the systems with spin-state transitions have not been touched upon in the study reported in Ref. 17. The most important question is the relation between the changes caused by varying the composition (increase of concentration y of the smaller rare-earth ions Eu) and that due to isotope substitution, and the physical mechanism underlying these changes. We see, *cf.* phase diagram in Ref. 17 and in Fig. 12 below, that there exists some correlation between these changes, but the situation is not so simple: thus, in the right part of the phase diagram the spin state transition increases both with the increase of Eu content y and with the increase of isotope mass (going from ^{16}O to ^{18}O). At the same time, in the left part of this phase diagram the effect of the increase of Eu content and of increasing oxygen mass on the phase transition (in this case transition to a nearly ferromagnetic state) is just the opposite: an increase in Eu content leads to the decrease of T_{FM}, but the increase of oxygen mass – to the increase of it.

Another important open question concerns the behavior of separate phases in the regime of phase separation. There are many different correlated systems, in which phase separation was detected in some range of compositions, temperatures, external fields, etc. Typically, the measured transition temperatures in this case changes e.g. with doping. However, it often remains unclear whether this change is the effect occurring in separate regions of different phases, or is just the result of averaging out over the inhomogeneous system. To answer these questions, we now carried out the detailed study of the behavior of the (PrEu)CoO_3, using as a tool the possibility of fine tuning the properties of the system by partial isotope substitution. This partial substitution plays in effect the same role as doping, external pressure, etc. The obtained results established the possibility of "rescaling" the changes in the system with doping and with isotope substitution and allowed us to clarify the questions formulated above.

As to the second question formulated above, just the possibility of fine tuning the properties of the system inside the region of phase separation, provided by partial isotope substitution, allowed us to study separately the behavior of different phases within this phase separated regime – the possibility, which would be very difficult to get by other means. Our results obtained in this way demonstrate that not only the average critical temperatures change with doping and with isotope substitution, but also "individual" transition temperatures (temperature of ferromagnetic transition in more metallic regions and the temperature of the spin-state transition in more insulating parts of the sample) do change with chemical and isotope composition.

As to the main, the first question formulated above, about the mechanisms governing the change of properties of the system with chemical and isotope composition, the experimental findings reported in the present paper provided us an opportunity to formulate a realistic theoretical model clarifying the mechanisms underlying the pronounced isotope effects in cobaltites exhibiting spin-state transitions. The theoretical analysis demonstrates that the main factor is the change of the effective bandwidth with the change both of chemical and isotope composition. The opposite trends in two parts of phase diagram mentioned above find natural explanation in this picture.

To analyze the effects of the partial oxygen isotope substitution for the doped cobaltites in the crossover region of the phase diagram, we have prepared a series of oxide materials with nearly continuous tuning of their characteristics. This allows us to trace the evolution of relative content of different phases as a function of $^{18}O/^{16}O$ ratio. Note that there were only few investigations of this kind, one of which we undertook earlier for $(La_{1-y}Pr_y)_{0.7}Ca_{0.3}MnO_3$ manganites.[18] Here, the pronounced isotope effect manifesting itself in $(Pr_{1-y}Eu_y)_{0.7}Ca_{0.3}CoO_3$ cobaltites provides indeed a unique possibility to address the problems discussed above through the use of the partial oxygen isotope substitution.

II. SAMPLES

Polycrystalline $(Pr_{1-y}Eu_y)_{0.7}Ca_{0.3}CoO_3$ samples were prepared by the chemical homogenization ("paper synthesis") method[19] through the use of the following operations. At first, non-concentrated water solutions of metal nitrates $Pr(NO_3)_3$, $Eu(NO_3)_3$, $Ca(NO_3)_2$, and $Co(NO_3)_2$ of 99.95% purity were prepared. The exact concentration of dissolved chemicals was established by gravimetric titration and, in the case of Co-based solution, by means of potentiometric titration. The weighted amounts of metal nitrate solutions were mixed in stoichiometric ratio and the calculated mixture of nitrates were dropped onto the ash-free paper filters. The filters were dried out at about 80°C and the procedure of the solutions dropping was performed repeatedly. Then, the filters were burned out and the remaining ash was thoroughly ground. It was annealed at 800°C for 2 hours to remove the carbon. The powder obtained was pressed into the pellets and sintered at 1000°C in the oxygen atmosphere for 100 hours. Finally, the samples were slowly cooled down to room temperature by switching off the furnace.

Samples were analyzed at room temperature by the powder X-ray diffraction using Cu K_α radiation. All detectable peaks were indexed by the space group, Pnma. According to the X-ray diffraction patterns, all $(Pr_{1-y}Eu_y)_{0.7}Ca_{0.3}CoO_3$ samples were obtained as single-phase crystalline materials.

We prepared a series of ceramic cobaltite samples with the degrees of enrichment by ^{18}O equal to 90%, 67%, 43%, 17%, and 0%. These values were determined by the changes in the sample mass in the course of the isotope exchange and by the mass spectrometry of the residual gas in the oxygen exchange contour. The samples were annealed in the appropriate ^{16}O–^{18}O gas mixture at 950 °C during 48 h at total pressure of 1 bar. The Eu doping of the samples was chosen to be near and on the both sides of the crossover doping level y_{cr}: a composition with the high Eu content exhibiting the SST, a low-Eu composition corresponding to the nearly ferromagnetic state, and the sample at the phase crossover, where both T_{SS} and T_{FM}, were observed. For all samples, we measured the temperature dependence of the real $\chi'(T)$ and imaginary $\chi''(T)$ parts of the ac magnetic susceptibility and electrical resistivity $\rho(T)$. The resistivity of the samples was measured by the conventional four-probe technique in the temperature range from 4.2 to 300 K . The measurements of ac magnetic susceptibility $\chi(T)$ were performed in ac magnetic field with a frequency 667 Hz and an amplitude of about 0.1 Oe. Based on these measurements, we were able to analyze the evolution the sample properties with the change Eu and ^{18}O content.

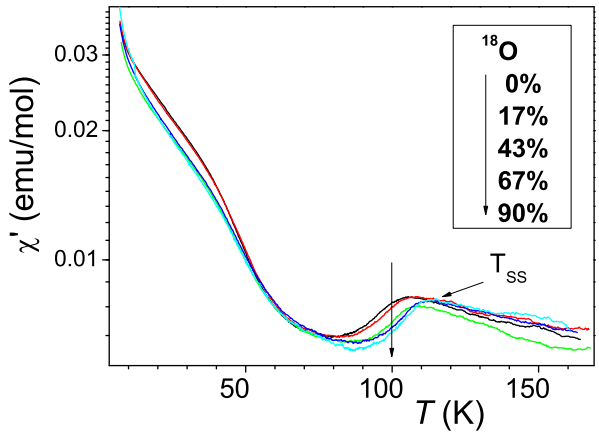

Figure 1: (Color online) Temperature dependence of magnetic susceptibility for $(Pr_{1-y}Eu_y)_{0.7}Ca_{0.3}CoO_3$ with $y = 0.2$.

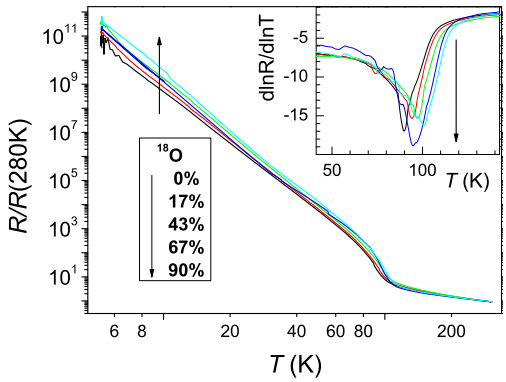

Figure 2: (Color online) Temperature dependence of electrical resistivity for $(Pr_{1-y}Eu_y)_{0.7}Ca_{0.3}CoO_3$ with $y = 0.2$.

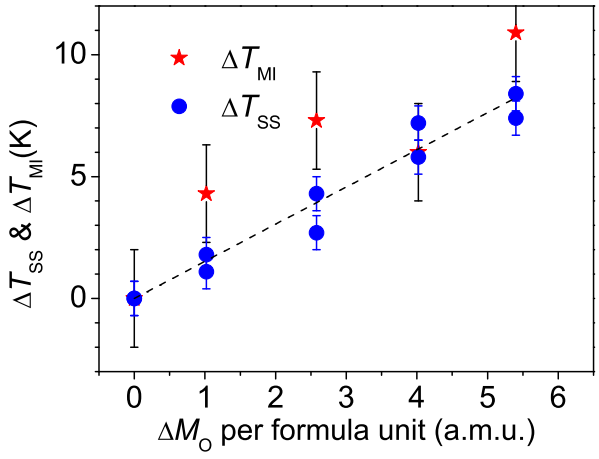

Figure 3: (Color online) Isotopic shift of the characteristic temperatures of the spin-state T_{SS} and metal-insulator T_{MI} transitions at the $^{16}O \rightarrow ^{18}O$ substitution for the sample with $y = 0.2$.

III. EXPERIMENTAL RESULTS

1. For the samples with $y > y_{cr}$ (Eu content $y = 0.20$), the material correspond to a "weakly-magnetic insulator", in notation of Ref. 17. The $\chi'(T)$ curves give clear indications of a spin-state transition (SST) at T_{SS} manifesting itself as a peak in the $\chi'(T)$, see Fig. 1. The value of T_{SS} increases with the ^{18}O content. The high-temperature phase is a paramagnet and a relatively good conductor, see Fig. 2. The low-spin (LS) insulating phase is dominant below the crossover to a LS state occurring at about 100 K. The increase of χ' at low temperatures is most probable caused by an incomplete transition, after which there may remain small magnetic (and presumably more conducting) clusters immersed into the LS state bulk insulator. As a result of this crossover to a LS state, the electrical resistance R increases by 10–12 orders of magnitude, which can be treated as a metal–insulator transition (MI), see Fig. 2). In these compounds, the metal–insulator transition is accompanied (or caused) by the SST. The ^{18}O content does not produce a significant effect on $R(T)$ at low T, although R is larger in the samples with heavy oxygen. The value of the metal–insulator transition temperature T_{MI} can be determined from the logarithmic derivative of $R(T)$, see inset of Fig. 2. The mass dependence of T_{MI} correlates well with the isotopic shift of T_{SS}, see Fig. 3. According to the calculation of isotopic constant $T \sim M^{-\alpha}$; $\alpha = -d\ln T/d\ln M = -(\Delta T/\Delta M)(M/T)$, we have the value α_{SS} and $\alpha_{MI} = -(1.5 \pm 0.07)$. The increasing in the oxygen mass promotes the development of the LS state.

2. The most important results are obtained for the samples with Eu content $y \sim y_{cr}$ ($y = 0.14$ and 0.16). They correspond to a wide concentration range of the phase separation.

For the sample with $y = 0.14$, we observe in $\chi'(T)$ curves a feature corresponding to a steep increase of the magnetization on cooling at 60–70 K, see Fig. 4. This behavior is caused by the FM phase arising in these samples. In addition, in the temperature dependence of resistivity, we see a steep increase of resistivity characteristic of the metal–insulator transition similar to that observed for the samples with $y = 0.2$, see Fig. 5. The transition temperature corresponds to the minimum in the logarithmic derivative of the resistivity, see inset of Fig. 5. This means that here we deal also with the change in the relative content of metallic and insulating phases suggesting the existence of the regions corresponding to the low-spin insulating state and the correlation between the metal–insulator and SS transitions. At the same time we do not observe any clear indications of the SST in the temperature dependence of the magnetic susceptibility. Thus, the samples with $y = 0.14$ turn out to be at the bound-

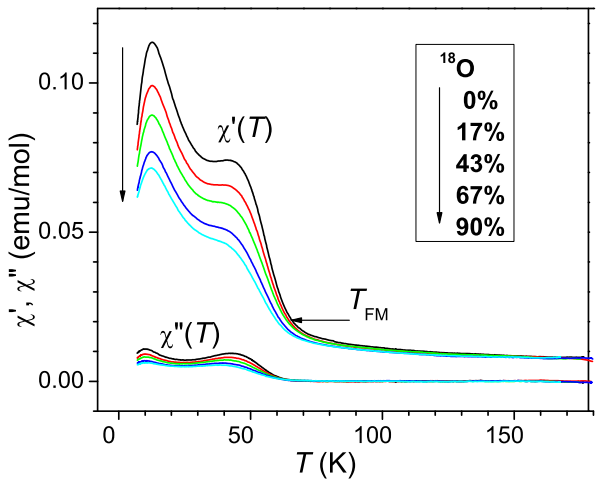

Figure 4: (Color online)Temperature dependence of magnetic susceptibility for $(Pr_{1-y}Eu_y)_{0.7}Ca_{0.3}CoO_3$ with $y = 0.14$.

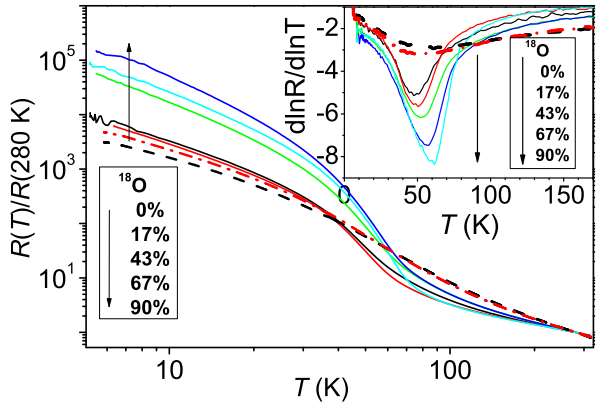

Figure 5: (Color online) Temperature dependence of electrical resistivity for $(Pr_{1-y}Eu_y)_{0.7}Ca_{0.3}CoO_3$ with $y = 0.14$ (solid line) and $y = 0.1$ with ^{16}O (dashed line) and ^{18}O (dash-dot line).

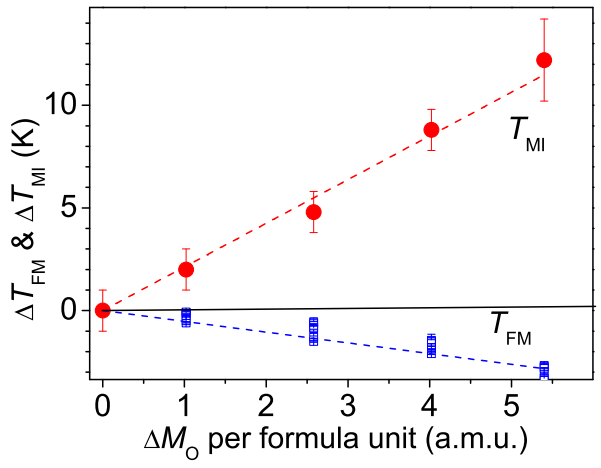

Figure 6: (Color online) Isotopic shift of the characteristic temperatures of the spin-state T_{SS}, metal-insulator T_{MI} and ferromagnetic T_{FM} transitions for the sample with $y = 0.14$.

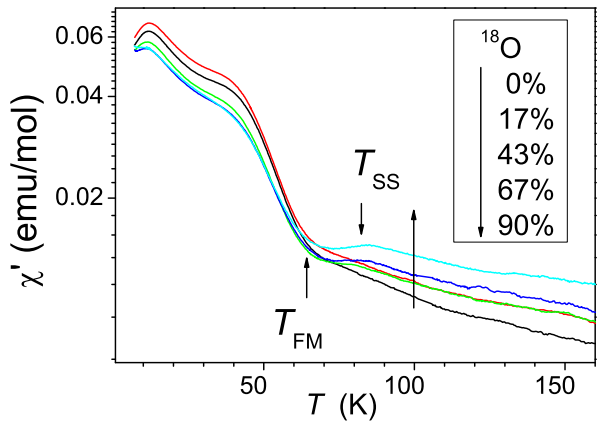

Figure 7: (Color online) Temperature dependence of magnetic susceptibility for $(Pr_{1-y}Eu_y)_{0.7}Ca_{0.3}CoO_3$ with $y = 0.16$.

ary of the phase separation range. The increasing in the oxygen mass favors the LS state as well as suppression of the FM phase and of the metallization.

The values of the isotopic constant calculated for the SS and FM transitions in this sample are $\alpha_{SS,MI} = -(1.7 \pm 0.06)$ and $\alpha_{FM} = (0.5 \pm 0.05)$, respectively. For this sample, the isotope shifts of the characteristic transition temperatures are illustrated in Fig. 6.

For the samples with $y = 0.16$, the effect of the partial oxygen isotope substitution by ^{18}O manifests itself even more clearly. Here, we observed the features characteristic both of FM and SS transitions. On the one hand, the temperatures dependence of χ' exhibits a steep growth at 60–70 K similar to that in the sample 0.14 indicating the existence of the FM transition. On the other hand, in of $\chi'(T)$, we observed a clearly pronounced peak, which can be attributed to SST at T_{SS} (Fig. 7). $\chi'(T)$ curves also demonstrate that the transition to the LS state gradually disappears with the decrease of the oxygen mass. In samples with small ^{18}O content ($< 17\%$), this transition is hardly seen due to the gradual transformation from the LS to FM state when the oxygen mass decreases. Note also that for $y = 0.16$ (as well as in the samples with $y = 0.14$) the temperature T_{FM} decreases with the growth of the average mass of oxygen.

In addition, the Curie–Weiss temperature θ in the formulas for the inverse magnetic susceptibility $\chi^{-1}(T)$ considerably decreases with the increase of the average mass of oxygen isotopes (see Fig. 8). For the samples with the largest oxygen mass, we have $\theta = 184$ K, whereas for the samples with the ^{16}O, $\theta = 45$ K. This phenomenon may be related to the transition from the antiferromagnetic interaction to ferromagnetic one.

For sample with $y = 0.16$ as well as in the samples with $y = 0.14$ and 0.2, we have found the growth of resistivity

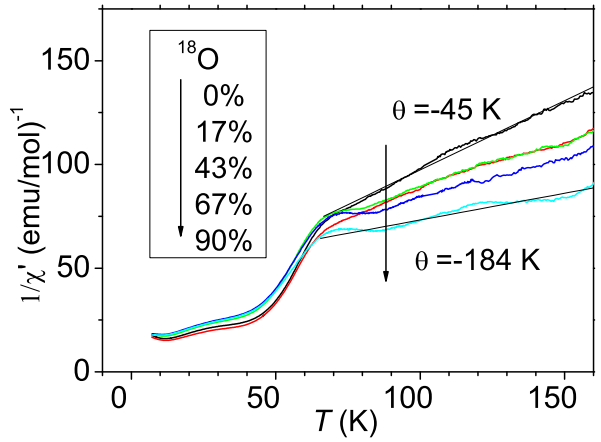

Figure 8: (Color online) Temperature dependence of inverse magnetic susceptibility for $(Pr_{1-y}Eu_y)_{0.7}Ca_{0.3}CoO_3$ with $y = 0.16$.

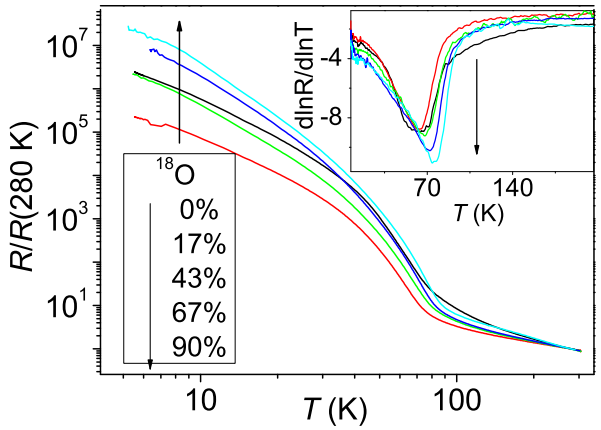

Figure 9: (Color online) Temperature dependence of electrical resistivity for $(Pr_{1-y}Eu_y)_{0.7}Ca_{0.3}CoO_3$ with $y = 0.16$.

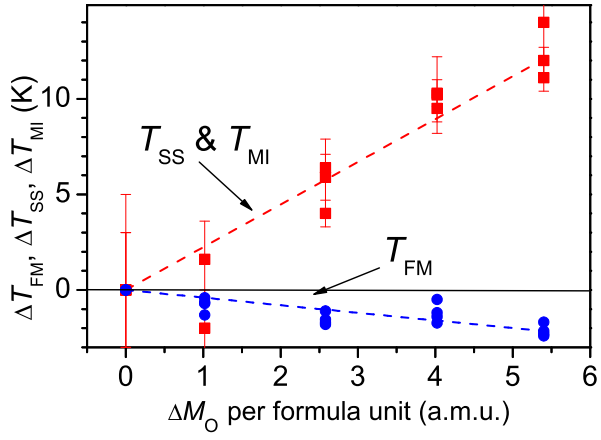

Figure 10: (Color online) Isotopic shift of the characteristic temperatures of the spin-state T_{SS}, metal-insulator T_{MI} and ferromagnetic T_{FM} transitions for the sample with $y = 0.16$.

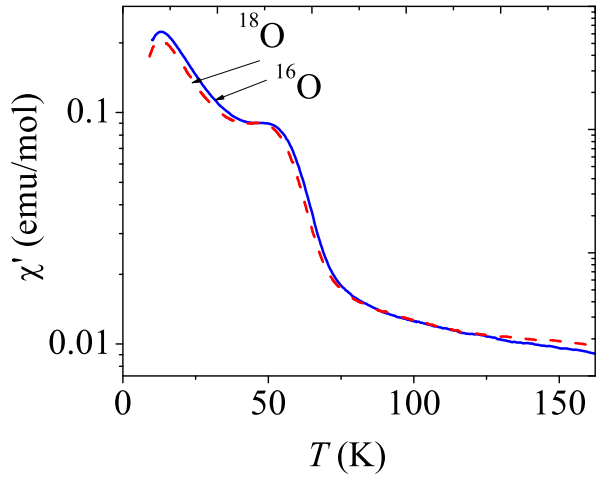

Figure 11: (Color online) Temperature dependence of magnetic susceptibility for $(Pr_{1-y}Eu_y)_{0.7}Ca_{0.3}CoO_3$ with $y = 0.1$.

at decreasing temperatures (by 5-7 orders of magnitude) and the metal-insulator transition in the vicinity of 70 K (Fig. 9). Both the resistivity and magnetic susceptibility data give clear indication that this sample is in the phase-separation range. The temperatures of MI and SS transitions increase with the average mass oxygen (see inset of Fig. 9). In the sample with $y = 0.16$, we see the same general tendency, namely the growth of T_{SS} and the decrease of T_{FM} with the growth of the average oxygen isotope mass. Here, the values of the isotope constant are $\alpha_{SS,MI} = -(1.7 \pm 0.06)$ and $\alpha_{FM} = (0.4 \pm 0.1)$, respectively; the isotope shifts of the characteristic transition temperatures are illustrated in Fig. 10.

3. Finally, the samples with $y < y_{cr}$ (Eu content $y = 0.10$) fall into the range of "nearly-metallic" ferromagnet. In Ref. 17, it was shown that at $T < T_{FM}$ the compositions with a low Eu content correspond to the domains of the metallic ferromagnetic phase embedded in a weakly magnetic nonconducting matrix.

According to the temperature dependence $\chi'(T)$ plotted in Fig. 11, the magnetization steeply increases on cooling at about $60 - 70$ K (i.e. the ferromagnetic phase arises). With the growth of the average oxygen mass, the value of $\chi'(T)$ decreases at low temperatures. Here, we have $T_{FM}(^{18}O) < T_{FM}(^{16}O)$ and the maximum isotope shift of T_{FM} does not exceed 2–3 K.

The electrical resistivity for this samples ($y = 0.10$) increases at low temperatures, even when the ferromagnetic phase arises. This behavior is quite similar to that observed in the samples with $y = 0.14$ and $y = 0.16$. Note that the electrical resistance in the samples with ^{18}O is higher than in those with ^{16}O. However, with the decrease of Eu content down to $y = 0.10$, the MI peculiarity in the resistance is suppressed. Such behavior $R(T)$ for samples with $y = 0.10$ can be compared with that for $y = 0.14$ samples, see Fig. 5) and inset of this

figure. The resistivity for samples $y = 0.10$ corresponds to a more smooth curve than for samples with $y = 0.14$, although the regular course of the temperature dependence remains nearly unchanged. Thus, the samples with $y = 0.10$ do not become really metallic but their behavior differs from the behavior of the samples with $y = 0.14$ (they do not exhibit indications of SST). Therefore, we argue that in the phase diagram, the composition with $y = 0.10$ lies outside the crossover region, on the left-hand side of it.

IV. DISCUSSION OF EXPERIMENTAL RESULTS

The obtained data for the temperatures of the phase transitions can be presented in the form of the phase diagram (Fig. 12). It illustrates that with the growth of Eu content the system transforms from the nearly ferromagnetic metal to the LS insulating state undergoing LS → IS spin-state transitions . Between these states, we have a broad crossover region corresponding to the phase separation. Indeed, the simultaneous observation both of T_{FM} and T_{SS} in the samples with Eu content $y = 0.14$ and 0.16 is a clear evidence of the phase separation in the system.

These samples also provide a spectacular illustration of the effect related to the variable content of ^{18}O. In particular, for the samples with $y = 0.16$, the temperature dependence of magnetic susceptibility (Fig. 4) exhibits at high values of ^{18}O content a pronounced feature corresponding to the SST. With the lowering of ^{18}O content, this feature becomes weaker and disappears below 17% of ^{18}O. Hence, we see that the change on the average oxygen mass can drastically affect the phase composition of the cobaltite samples.

The oxygen isotope substitution ^{16}O →^{18}O shifts the phase equilibrium toward the insulating state. For the heavier isotope, the spin-state transition temperature T_{SS} grows, while the ferromagnetic transition temperature T_{FM} decreases. The change of average oxygen mass is a unique tool for investigating special properties of phase separation in cobaltites near the crossover between the FM and LS phases. We also see that the effect of increasing ^{18}O content on the system is similar to that of increasing Eu content.

The analysis of these results for different chemical and isotope composition demonstrates that the effect of the increase in Eu content y and of average oxygen mass are qualitatively similar. One can rescale the dependence of the transition temperature on both parameters using the combined variable $y + 0.01x$, where x is the relative content of ^{18}O, as shown in Fig. 13. Both the temperatures of SS and FM transitions depend almost linearly on this combined variable. We see that the change of Eu content by 1% is equivalent to the change of the isotope content by 100 % . This actually the most important result of the present study. The theoretical analysis of these results is given in the following sections.

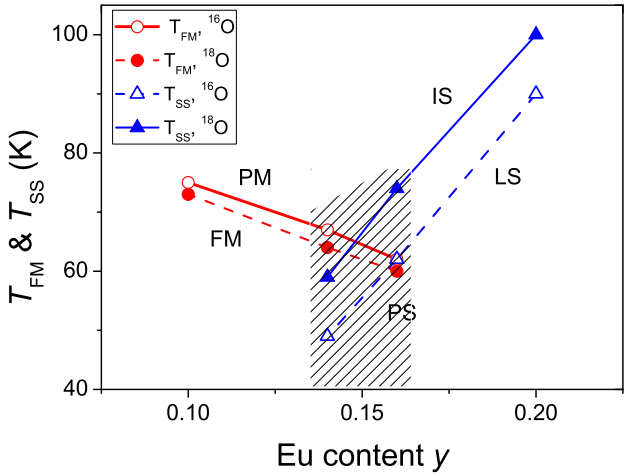

Figure 12: (Color online) Phase diagram of $(Pr_{1-y}Eu_y)_{0.7}Ca_{0.3}CoO_3$ compound with ^{16}O and 90% ^{18}O. PM, FM, IS, and LS stand for the paramagnetic, ferromagnetic, intermediate-spin, and low-spin state, respectively. The hatched area corresponds to the phase-separated state (PS).

V. CALCULATION DETAILS

To explain the composition and isotope dependence of the properties of our system (see Fig. 12), especially the similar dependence of the SST temperature and the temperature of the FM transition illustrated in Fig. 13, we propose a realistic model (Section VII) based predominantly on the change of the electron bandwidth with chemical and isotope composition. Some input, as well as the estimates of relevant parameters are taken from the *ab initio* band structure calculations for the limiting "pure" compositions corresponding to $y = 0$ ($PrCoO_3$) and $y = 1$ ($EuCoO_3$).

The crystal structure of $PrCoO_3$ obtained in Ref. 22 for $T = 300$ K was utilized in those calculations. For $EuCoO_3$, the lattice parameters were taken from Ref. 23. The exact atomic positions for $EuCoO_3$ are unknown, therefore we used the same positions as for $PrCoO_3$ (with the correct unit cell volume for $EuCoO_3$). The splitting between different one-electron energy levels Δ_{CF} was calculated within the local density approximation (LDA) in the framework of the linear muffin-tin orbitals method (LMTO).[24] Partially filled, but physically unimportant $4f$ states of the Eu and Pr were treated as frozen.[25]

The Brillouin-zone (BZ) integration in the course of self-consistency iterations was performed over a mesh of 144 **k**-points in the irreducible part of the BZ.

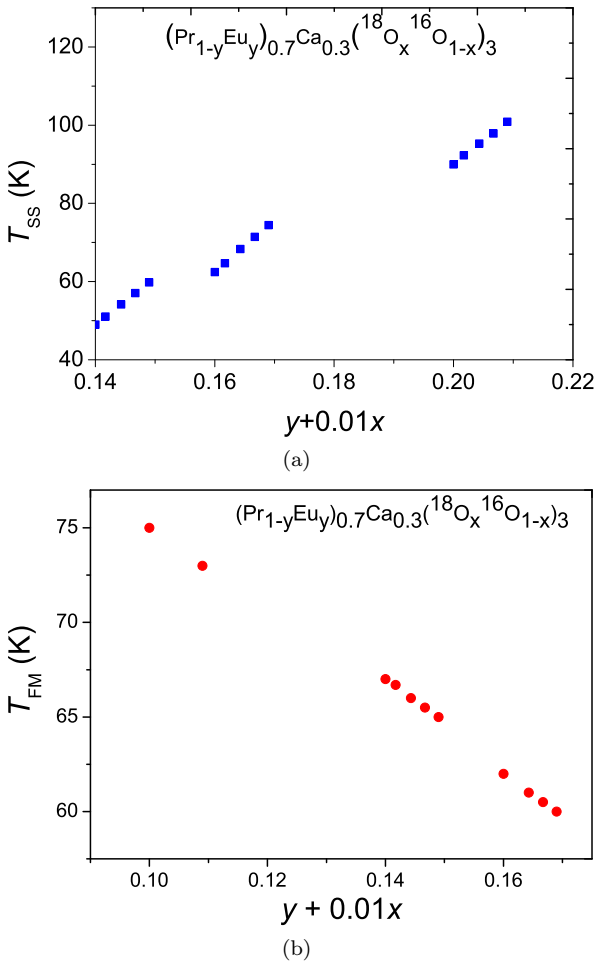

Figure 13: (Color online) Plots illustrating the combined effect of the Eu and ^{18}O doping on the temperature of spin-state transition T_{SS} and on the ferromagnetic transition temperature T_{FM}. Note the difference of the temperature scales in panels (a) and (b).

VI. DOPING DEPENDENCE: LDA RESULTS

There are different ways to estimate the temperature of the spin-state transition with the use of the band structure calculation. The most direct way is to calculate the total energies of different spin states.[20,21]. However, in the case of the doped system this would require very large supercells. Moreover, currently,we have no single commonly accepted model, which can explain all experimental facts. Various combinations of a static or dynamic order of the different spin states are discussed in the literature.[25,39–42] This is the reason why we chose an alternative approach.

The energy of any of the spin states depends on two important parameters: the single-electron energy difference Δ_{CFS} between the highest t_{2g} and the lowest e_g levels, and the intra-atomic Hund's rule exchange coupling J_H. The Hund's rule energy J_H is an atomic characteristic and does not change appreciably either with the Eu doping or with the isotope substitution. So,to investigate the dependence of the spin-state transition temperature on the doping or isotope substitution in the first approximation one can focus on the study of the single parameter, Δ_{CFS}. If Δ_{CFS} is large enough ($\Delta_{CFS} > 2J_H$), it will be energetically favorable to localize all electrons in the low-lying t_{2g} subshell of Co^{3+}, i.e. the system will be in the low-spin state. With decrease of the crystal-field splitting, some electrons can be transferred to e_g subshell, which allows the system to gain the exchange energy, since there will be more electrons with the same spin. As we will show below both the isotope substitution and the doping can be related to the crystal-field splitting.

In order to estimate Δ_{CFS}, we used the Wannier function projection procedure proposed in Ref. 26, which allows us to project the full-orbital band Hamiltonian onto the subspace of few states (five d states of Co). With the Fourier transformation one obtains the Hamiltonian in the real space, from which the splitting between highest in energy t_{2g} and lowest e_g can be easily calculated. For $PrCoO_3$, we obtain $\Delta_{CFS} = 2.07$ eV.

The total and partial densities of states (DOS) obtained for $PrCoO_3$ in the LDA calculations are presented in Fig. 14. In the octahedral symmetry, the $3d$ states of Co are split into t_{2g} and e_g subbands. In the LDA, the valence band is mostly formed by the Co$-t_{2g}$ states, while the conduction band is determined by the Co$-e_g$ states. The O$-2p$ band is located in the energy range from -7 to -1.5 eV.

The DOS for $EuCoO_3$ is qualitatively very similar and corresponding calculations of Δ_{CFS} result in the value of 2.14 eV. The increase of the $t_{2g} - e_g$ excitation energy on going from $PrCoO_3$ to $EuCoO_3$ is caused by two factors. The first is the lanthanide contraction: the substitution of the large Pr^{3+} by smaller Eu^{3+} ions leads to some decrease of the Co–O distance and to the corresponding increase in the $p - d$ hybridization, which leads to an increase of the difference between the centers of the t_{2g} and e_g bands. The second effect is related to the decrease of the effective widths of t_{2g} and e_g energy bands with the corresponding increase of the energy gap between them. This narrowing of energy bands on going from $PrCoO_3$ to $EuCoO_3$ is also related, in effect, with the lanthanide contraction, because of which the tilting of CoO_6 octahedra increases and the Co–O–Co angle and the corresponding bandwidth decrease on going from $PrCoO_3$ to $EuCoO_3$. Both these effects finally lead to the increase of Δ_{CFS} with Eu content, which leads to the enhanced stabilization of of the LS state of Co^{3+} (see the more detailed discussion of these effects in Section VII).

This change of the crystal-field splitting (CFS) results in the modification of the spin-state transition temperature, since this transition is due to the competition of the Hund's rule exchange coupling J_H and the CFS.[25]

It was found in Refs. 17 and 27 (see also Fig. 12) that the change of the Eu content y in $(Pr_{1-y}Eu_y)_{0.7}Ca_{0.3}CoO_3$ by 0.02 leads to the change of

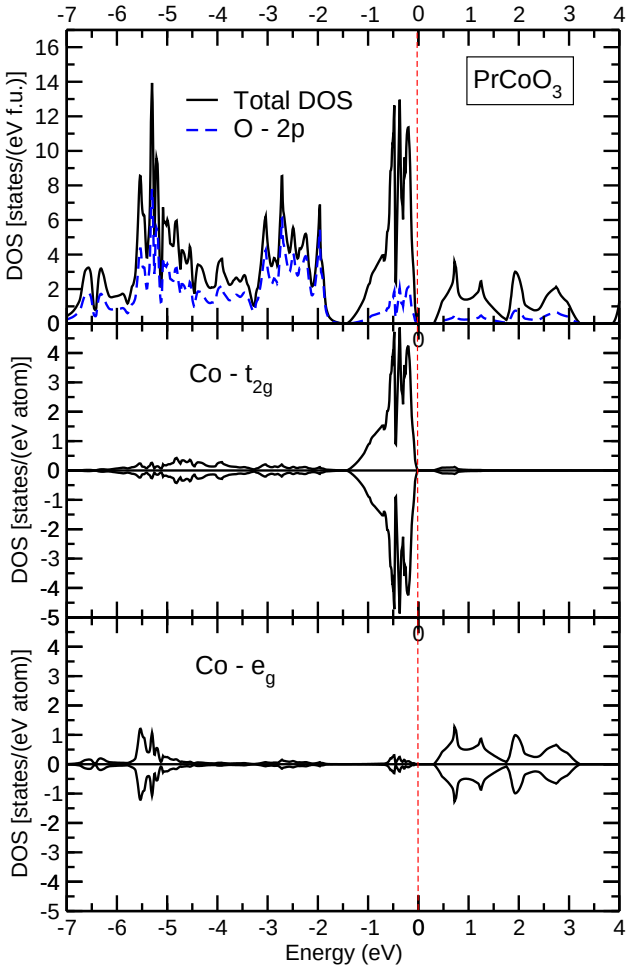

Figure 14: (Color online) The total and partial densities of states (DOS) for $PrCoO_3$. The Fermi energy corresponds to zero.

the spin-state transition temperature by about 14 K. In the first approximation, it is possible to neglect the presence of Ca and interpolate the change of the CFS for the complex system like $(Pr_{1-y}Eu_y)_{0.7}Ca_{0.3}CoO_3$ using the values of the CFS for $y = 1$ ($PrCoO_3$) and $y = 0$ ($EuCoO_3$). Such a linear interpolation predicts the change of the spin-state transition temperature by 16 K, if y changes by 0.02, which is in an excellent agreement with the experiment.[17,27]

VII. ISOTOPE SUBSTITUTION: MODEL RESULTS

The isotope substitution does not change the chemical properties of the ions such as the oxidation numbers or bonding energies. However, it affects the crystal lattice through the modification of the phonon spectra. Below, following the approach of Ref. 28, we demonstrate the effect of this modification on the electronic and magnetic properties and hence on the spin-state transition.

In the tight-binding model, the band spectra of a solid is determined by the on-site ionic energy levels ε_i^{nlm} and the hopping matrix elements between different sites $t_{ij}^{ll',mm'}$. The ionic energies ε_i^{nlm} obviously do not depend on the mass of the ions, being determined by the quantum numbers and the intra-atomic Coulomb and exchange interactions. The hopping parameters depend on the type of the orbitals (s, p, d, f), bonding type (π, σ, δ), and the distance between ions, u. According to the famous Harrison parametrization[29,30] in the absence lattice vibrations the hopping integrals between e.g. p orbitals of the oxygen and transition metal d-orbitals equal to

$$t_{pd} = \frac{C_{pdm}}{u^4}, \tag{1}$$

where coefficients C_{pdm} depend on the type of the bonding and can be different for different metals and ligands.[29,31]

The static version of Eq. (1) can be generalized taking into account the presence of lattice vibrations, i.e. phonons, which depend on the ion masses. The mean pd hopping matrix element can be calculated as

$$\begin{aligned}\langle t_{pd}\rangle &= \frac{1}{2v}\int_{u_0-v}^{u_0+v}\frac{C_{pdm}}{u^4}du = \\ &= \frac{C_{pdm}}{6v}\Big(\frac{1}{(u_0-v)^3} - \frac{1}{(u_0+v)^3}\Big),\end{aligned} \tag{2}$$

where $v = \sqrt{\langle \delta u^2\rangle}$ is the mean square displacement from the equilibrium position u_0 due to phonons. Since $v/u_0 \ll 1$ one may simplify last equation expanding it to series to the 4th order

$$\langle t_{pd}\rangle = \frac{C_{pdm}}{u_0^4}\Big(1 + \frac{10}{3}\Big(\frac{v}{u_0}\Big)^2\Big) + O(\Big(\frac{v}{u_0}\Big)^4). \tag{3}$$

In the static limit $v \to 0$, the last formula coincides with Eq. (1).

In the Debye model at zero temperature, the mean square displacement is written as[32]

$$v = \sqrt{\langle \delta u^2\rangle} = \frac{9\hbar^2}{4k_B\theta_D}\frac{1}{m}. \tag{4}$$

Here m is the mass of vibrating ions and θ_D is the Debye temperature. Due to different mass the mean square displacement in the compounds enriched by ^{16}O or ^{18}O will be different. The Debye temperature for the very similar system, $LaCoO_3$ was found to be ~600 K.[33]. One may use this value to estimate v in $(Pr_{1-y}Eu_y)_{0.7}Ca_{0.3}CoO_3$. Then the mean square displacement for ^{18}O is $v_{18} = 0.100$ Å and $v_{16} = 0.107$ Å for ^{16}O. According to Eq. (3), this leads to the decrease of the effective bandwidth in going from ^{16}O to ^{18}O. Qualitative explanation of this effect is presented in Fig. 15a. For strong electron-phonon coupling the same effect could be attributed to polaron band narrowing depending on the isotope mass.

The temperature of the spin-state transition depends on the energy difference between t_{2g} and e_g subbands, which is defined by the widths of corresponding bands and the positions of their centers. We start with the study of the bandwidths dependence on the ligand ion mass, see schematic illustration in Fig. 15b.

In order to calculate the change in the bandwidth caused by the $^{16}O \rightarrow {}^{18}O$ substitution, one needs to know the hopping integrals, which depend on two unknown parameters C_{pdm} and u_0. The C_{pdm} coefficients can be in principle evaluated as it is prescribed for instance in Ref. 29. However, for the better precision we calculated C_{pdm} parameters from the LDA t_{2g} and e_g bandwidths in pure $PrCoO_3$. The equilibrium Co–O distance u_0 in its turn can be evaluated from the actual crystal structure data for $EuCoO_3$ and $PrCoO_3$.

Finally, performing all these calculations, one gets that the t_{2g} bandwidth decreases on 22 K when one substitutes ^{16}O by ^{18}O. The decrease of the e_g bandwidth is two times larger and equals 44 K. In effect, the minimum energy of the $t_{2g} \rightarrow e_g$ transition increases by 33 K. Hence the spin-state transition temperature due to the change of the bandwidth must increase by the same value going from ^{16}O to ^{18}O in qualitative accordance with the experiment.[17]

Let us consider the second mechanism, which affects the spin-state transition and which is related to the dependence of changes in the centers of gravity of corresponding bands (i.e. crystal-field splitting) with the isotope substitution. It turns out the this effect counteracts the first one(change of the effective t_{2g} and e_g bandwidths), but numerically this second effect is much smaller, see below. Generally speaking, there are two main contributions to the crystal-field splitting, Δ_{CFS}. One comes from the Coulomb interaction of the $3d$ electrons with the negatively charged ligands, another is due to the hybridization between d orbitals of metal ions metal and p orbitals of the ligands.[34,35] For most oxides of $3d$ transition metals both terms are acting in "the same direction", resulting to the same sequence of levels.[36] That is why so crude approaches as the atomic sphere approximation (ASA)[37] often used in the *ab initio* calculations provide quite precise band structure in most cases. The effect of the Coulomb term can be omitted or effectively incorporated into the kinetic energy contribution. Below we will follow the same strategy by considering the kinetic energy only, keeping in the mind that the Coulomb contribution can be taken into account via the parameters renormalization.

In the second order of the perturbation theory, the crystal-field splitting between t_{2g} and e_g subbands is written as

$$\Delta_{CFS} = \frac{t_{pd\sigma}^2 - t_{pd\pi}^2}{\Delta_{CT}}, \qquad (5)$$

where Δ_{CT} is the charge-transfer energy (which corresponds to the $d^n p^6 \rightarrow d^{n+1} p^5$ transition), $t_{pd\sigma}$ and $t_{pd\pi}$ are the hopping matrix elements for different types of the bonds.

Since the average hopping $\langle t_{pd} \rangle$ decreases on going from ^{16}O to ^{18}O according to Eqs. (3) and (4), the crystal-field splitting should also decrease as follows from Eq. (5). As a result, this contribution should lead to the opposite tendency: decrease of the spin-state transition temperature going from ^{16}O to ^{18}O. However, this effect does not exceed few kelvins, at the realistic values of the charge-transfer energy in cobaltites.[38]

Note also that we estimated here the changes in the distance between the *edges* of t_{2g} and e_g subbands. However, at finite temperatures, we should have not only the transitions between the band edge but just from one subband to another. Such a temperature-induced smearing could diminish somehow our estimates of the isotope effect in SST.

In Fig. 13b, we see that the isotope effect for T_{FM}, being much weaker (than for T_{SS}), is of the opposite sign. Nevertheless, there is the same similarity between the effects of the Eu content and the oxygen isotope substitution. This is in agreement with our expectations, because the ferromagnetism of the low-Eu doped samples with metallic clusters should be stabilized by the double-exchange mechanism, according to which T_{FM} is proportional to the effective bandwidth of the itinerant electrons. This bandwidth decreases for the heavier isotope, that is why T_{FM} goes down at the $^{16}O \rightarrow {}^{18}O$ substitution as well as at increasing Eu content, see Fig. 13b. A schematic illustration of the mechanism underlying the oxygen isotope effect discussed above is given in Fig. 15.

VIII. CONCLUSIONS

Experimental studies carried out for $(Pr_{1-y}Eu_y)_{0.7}Ca_{0.3}CoO_3$ cobaltites with varying isotope substitution of ^{16}O by ^{18}O demonstrated that there exists a strong similarity in the changes caused by the chemical composition (increasing Eu content) and those arising from the oxygen isotope substitution. The chemical composition $y \sim 0.1 - 0.2$ was chosen because in this range a crossover occurs between the ferromagnetic near-metallic state with magnetic Co ions to the nonmagnetic insulator with the low-spin Co^{3+} ($t_{2g}^6 e_g^0$, $S = 0$), see Fig. 12.

The main experimental conclusion presented in Fig. 13 is that one can rescale the behavior of this system. The dependence of the spin-state transition temperature and of the ferromagnetic transition temperature on content y of Eu and on the content x of the heavier isotope ^{18}O can be represented by the same almost linear plot as function of the combined variable $y + 0.01x$. This means, for example, that the change of Eu content y by 0.005 is equivalent to the substitution of 50% of ^{16}O by ^{18}O. In addition, it clearly demonstrates that not only the average transition temperatures change with doping and with isotope substitution, but also the transition temperatures for each separate phase vary with chemical and isotope

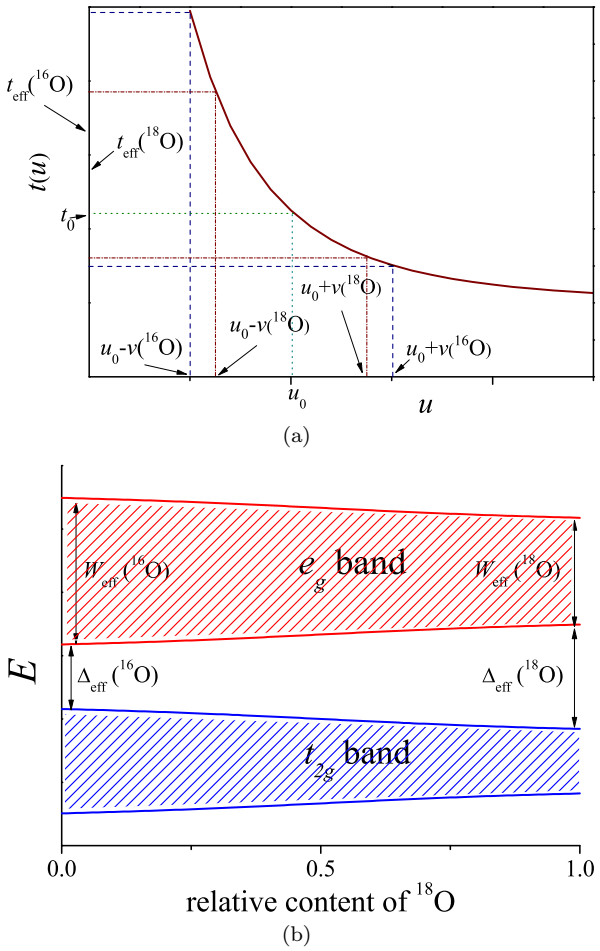

Figure 15: (Color online) Schematic illustration of the effects of oxygen isotope substitution (a) on the effective hopping integral t_{eff} and (b) on the effective gap Δ_{eff} between the e_g and t_{2g} bands and on the effective width W_{eff} of the e_g band. Solid curve in panel (a) depicts the hopping integral t as function of interion distance u according to Eq. (1). Effective hopping integrals t_{eff} are determined by averaging $t(u)$ over the interval given by the mean square displacement v of ions due to the lattice vibrations (4) (crudely, $t_{eff} = 1/2[t(u_0 + v) + t(u_0 - v)]$ for each isotope). We see that $t_{eff}(^{16}O) > t_{eff}(^{18}O)$. As a result, $\Delta_{eff}(^{18}O) > \Delta_{eff}(^{16}O)$ and hence $T_{SS}(^{18}O) > T_{SS}(^{16}O)$. At the same time, $W_{eff}(^{18}O) < W_{eff}(^{16}O)$ and hence $T_{FM}(^{18}O) < T_{FM}(^{18}O)$.

composition.

Based on this similarity between the role of chemical and isotope composition for the spin-state transition and for the transition to the ferromagnetic state at a smaller Eu content, we propose a theoretical explanation of the isotope effect in these transitions. We investigate the corresponding changes and estimate the relevant parameters using the *ab initio* band structure calculations. These results together with the analytical model allow us to explain the observed behavior. In particular, the isotope effect both in the spin-state and ferromagnetic transitions is interpreted in terms of the change in the corresponding widths of the d bands occurring due to the electron-phonon renormalization, which depends on the atomic masses of the respective isotopes.

All this demonstrates once again that the oxygen isotope substitution is a powerful tool for revealing salient features in the behavior of strongly correlated magnetic oxides.

Summarizing, we can say that using this approach, we established, first, that in the aforementioned crossover range, we can clearly distinguish two coexisting phases, nearly insulating exhibiting a spin-state transition and nearly metallic "ferromagnetic", with the different behavior of the transition temperatures. Second, we have found that these transition temperatures depend almost linearly on the content of the heavy oxygen isotope, which is a non-trivial observation clearly demonstrating that the electronic structure could be effectively controlled by isotopes. Third, based on these observations and using the parameters deduced from our band-structure calculations, we put forward a simplified model capturing the main physics of the isotope effect in the systems with spin-state transitions and quantitatively describing the experimental data.

Acknowledgments

This work is supported by the Russian Foundation for Basic Research (projects 10-02-00140-a, 10-02-00598-a, 10-02-96011-a, 11-02-00708-a, and 11-02-91335-NNIO-a), by the Ural Branch of Russian Academy of Sciences through the young-scientist program, by the German projects SFB 608, DFG GR 1484/2-1, FOR 1346, and by the European network SOPRANO.

[1] N. A. Babushkina, L. M. Belova, O. Yu. Gorbenko, A. R. Kaul, A. A. Bosak, V. I. Ozhogin, K. I. Kugel, Nature **391**, 159 (1998).
[2] J. B. Goodenough and P. M. Raccah, J. Appl. Phys. **36**, 1031 (1965).
[3] K. Asai, A. Yoneda, O. Yokokura, J. M. Tranquada, G. Shirane, and K. Kohn, J. Phys. Soc. Jpn. **67**, 290 (1998).
[4] T. Saitoh, T. Mizokawa, A. Fujimori, M. Abbate, Y. Takeda, and M. Takano, Phys. Rev. B **55**, 4257 (1997).
[5] Y. Tokura, Y. Okimoto, S. Yamaguchi, H. Taniguchi, T. Kimura, and H. Takagi, Phys. Rev. B **58**, R1699 (1998).
[6] M. A. Korotin, S. Y. Ezhov, I. V. Solovyev, V. I. Anisimov, D. I. Khomskii, and G. A. Sawatzky, Phys. Rev. B **54**, 5309 (1996).
[7] K. Berggold, M. Kriener, P. Becker, M. Benomar, M. Reuther, C. Zobel, and T. Lorenz, Phys. Rev. B **78**, 134402

(2008).
[8] N. B. Ivanova, S. G. Ovchinnikov, M. M. Korshunov, I.M. Eremin, and N. V. Kazak, Usp. Fiz. Nauk. **179**, 837 (2009) [Physics - Uspekhi **52**, 789 (2009)].
[9] R. Ganguli, A. Maignan, C. Martin, M. Hervieu, and B. Raveau, J. Phys.: Condens. Matter **14**, 8595 (2002).
[10] J. Wu and C. Leighton, Phys. Rev. B **67**, 174408 (2003).
[11] D. Phelan, Despina Louca, K. Kamazawa, S.-H. Lee, S. Rosenkranz, M. F. Hundley, J. F. Mitchell, Y. Motome, S. N. Ancona, and Y. Moritomo, Phys. Rev. Lett. **97**, 235501 (2006).
[12] A. Podlesnyak, M. Russina, A. Furrer, A. Alfonsov, E. Vavilova, V. Kataev, B. Buchner, Th. Strassle, E. Pomjakushina, K. Conder, and D. I. Khomskii, Phys. Rev. Lett. **101**, 247603 (2008).
[13] A. O. Sboychakov, K. I. Kugel, A. L. Rakhmanov, and D. I. Khomskii, Phys. Rev. B **80**, 024423 (2009)
[14] J. Yu, Despina Louca, D. Phelan, K. Tomiyasu, K. Horigane, and K. Yamada, Phys. Rev. B **80**, 052402 (2009).
[15] S. El-Khatib, Shameek Bose, C. He, J. Kuplic, M. Laver, J. A. Borchers, Q. Huang, J. W. Lynn, J. F. Mitchell, and C. Leighton, Phys. Rev. B **82**, 100411 (2010).
[16] A. Podlesnyak, G. Ehlers, M. Frontzek, A. S. Sefat, A. Furrer, Th. Strassle, E. Pomjakushina, K. Conder, F. Demmel, and D. I. Khomskii, Phys. Rev. B **83**, 134430 (2011).
[17] A. V. Kalinov, O. Yu. Gorbenko, A. N. Taldenkov, J. Rohrkamp, O. Heyer, S. Jodlauk, N. A. Babushkina, L. M. Fisher, A. R. Kaul, A. A. Kamenev, T. G. Kuzmova, D. I. Khomskii, K. I. Kugel, and T. Lorenz, Phys. Rev. B **81**, 134427 (2010).
[18] N. A. Babushkina, A. N. Taldenkov, L.M. Belova, E. A. Chistotina, O. Yu. Gorbenko, A. R. Kaul, K. I. Kugel, and D. I. Khomskii, Phys. Rev. B **62**, R6081 (2000).
[19] A. M. Balagurov, V. Yu. Pomjakushin, D. V. Sheptyakov, V. L. Aksenov, N. A. Babushkina, L. M. Belova, A. N. Taldenkov, A. V. Inyushkin, P. Fischer, M. Gutmann, L. Keller, O. Yu. Gorbenko, and A. R. Kaul, Phys. Rev. B **60**, 383 (1999); O. Yu. Gorbenko, O. V. Melnikov, A. R. Kaul, A. M. Balagurov, S. N. Bushmeleva, L. I. Koroleva, and R. V. Demin, Mater. Sci. Eng. B **116**, 64 (2005).
[20] S. V. Streltsov and N. A. Skorikov, Phys. Rev. B **83**, 214407 (2011).
[21] M. A. Korotin, S. Yu. Ezhov, I. V. Solovyev, V. I. Anisimov, D. I. Khomskii, and G. A. Sawatzky, Phys. Rev. B **54**, 5309 (1996).
[22] K. Knížek, J. Hejtmánek, Z. Jirák, P. Tomeš, P. Henry, and G. André, Phys. Rev. B **79**, 134103 (2009).
[23] J. Baier, S. Jodlauk, M. Kriener, A. Reichl, C. Zobel, H. Kierspel, A. Freimuth, and T. Lorenz, Phys. Rev. B **71**, 014443 (2005).
[24] O. K. Andersen and O. Jepsen, Phys. Rev. Lett. **53**, 2571 (1984).
[25] I. A. Nekrasov, S. V. Streltsov, M. A. Korotin, and V. I. Anisimov, Phys. Rev. B **68**, 235113 (2003).
[26] S. V. Streltsov, A. S. Mylnikova, A. O. Shorikov, Z.V. Pchelkina, D. I. Khomskii, and V. I. Anisimov, Phys. Rev. B **71**, 245114 (2005).
[27] N. Babushkina, A. Taldenkov, A. Kalinov, L. Fisher, O. Gorbenko, T. Lorenz, D. Khomskii, and K. Kugel, Zh. Eksp. Teor. Fiz. **138**, 215 (2010) [JETP **111**, 189 (2010)].
[28] N. A. Babushkina, L. M. Belova, V. I. Ozhogin, O. Yu. Gorbenko, A. R. Kaul, A. A. Bosak, D. I. Khomskii, and K.I. Kugel, J. Appl. Phys. **83**, 7369 (1998).
[29] W. Harrison, *Elementary Electronic Structure* (World Scientific, Singapore, 1999).
[30] O. Andersen and O. K. Jepsen, Physica B **91**, 317 (1977).
[31] J. C. Slater and G. F. Koster, Phys. Rev. **94**, 1498 (1954).
[32] J. Reissland, *The Physics of Phonons* (Wiley, New York, 1973).
[33] S. Stølen, F. Grønvold, H. Brinks, T. Atake, and H. Mori, Phys. Rev. B **55**, 14103 (1997).
[34] C. Ballhausen, *Introduction to Ligand Field Theory* (McGraw-Hill, New York, 1962).
[35] H. Sugano, S. Tanabe, and Y. Kamimura, *Multiplets of Transition-Metal Ions in Crystals* (Academic Press, New York, 1970).
[36] A. Ushakov, S. V. Streltsov, and D. I. Khomskii, J. Phys.: Condens. Matter **23**, 445601 (2011).
[37] H. Skiver, *The LMTO Method* (Springer-Verlag, Berlin, 1984).
[38] A. Chainani, M. Mathew, and D. D. Sarma, Phys. Rev. B **46**, 9976 (1992).
[39] K. Knížek, Z. Jirák, J. Hejtmánek, P. Novák, and W. Ku, Phys. Rev. B **79**, 014430 (2009).
[40] Y. Ren, J.-Q. Yan, J.-S. Zhou, J. B. Goodenough, J. D. Jorgensen, S. Short, H. Kim, T. Proffen, S. Chang, and R. J. McQueeney, Phys. Rev. B **84**, 214409 (2011).
[41] M. W. Haverkort, Z. Hu, J. C. Cezar, T. Burnus, H. Hartmann, M. Reuther, C. Zobel, T. Lorenz, A. Tanaka, N. B. Brookes, H. H. Hsieh, H.-J. Lin, C. T. Chen, and L. H. Tjeng, Phys. Rev. Lett. **97**, 176405 (2006).
[42] K. V. Lamonova, E. S. Zhitlukhina, R. Yu. Babkin, S. M. Orel, S. G. Ovchinnikov, and Y. G. Pashkevich, J. Phys. Chem. A **115**, 13596 (2011).